Application of Intelligent Models in Investigating the Energy Dissipation in Labyrinth Weirs with Various Cycles Form

Hamidreza Abbaszadeh [*,1], Reza Tarinejad [1], John Abraham [2]

1. Faculty of Civil Engineering, University of Tabriz, Tabriz, Iran.
2. School of Engineering, University of St. Thomas, St. Paul, MN 33901, USA

***Corresponding Author:**
Hamidreza Abbaszadeh

Email: ha.abbaszadeh@tabrizu.ac.ir
Received: 2024.11.14
Accepted: 2025.02.21
J. Hydraul. Struct., 2025; 11(4):16-32
DOI: 10.22055/jhs.2025.48309.1329

ABSTRACT

Weirs play a crucial role as hydraulic structures in the regulation and control of water flow. This study investigates the relative energy dissipation in labyrinth weirs, examining various configurations, scales, and cycle types, using advanced computational models like Support Vector Machine (SVM), Random Forest (RF), and Artificial Neural Network (ANN). In SVM modelling, the results from different kernel functions reveal that the Radial Basis Function (RBF) kernel outperforms polynomial, linear, and sigmoid kernels in predicting relative energy dissipation. For the RBF kernel, the statistical metrics were found to be (R=0.907), (Mean RE%=1.38), (RMSE=0.0153), and (KGE=0.744) in test phase. where RE, Mean RE, RMSE and KGE represent the Relative Error, Mean Relative Error, Root Mean Square Error and Kling Gupta Efficiency, respectively. In contrast, in the ANN model, the multilayer perceptron (MLP) network showed higher accuracy than the RBF network, achieving 0.969, 0.73%, 0.007, and 0.968 for the same indicators. For the RF model, these values were recorded as 0.878, 1.78%, 0.0192, and 0.362, respectively. Comparative analysis indicates that the ANN model offers superior predictive performance over SVM and RF models. Additionally, non-linear polynomial regression equations, derived from dimensionless parameters, are proposed for estimating relative energy dissipation. Notably, single-cycle weirs exhibited the greatest energy dissipation among the configurations studied.

KEYWORDS

Energy dissipation, Labyrinth weirs, Soft computing, Weir cycle.

1. Introduction

When discussing flow control structures, weirs represent one of the most significant types. Weirs commonly used for measuring flow, regulating flow levels, and controlling the flow of irrigation and drainage channels. Labyrinth weirs are used in increase efficiency. The amount of flowing passes over the weirs during the flood peak is significant, so the presence of a weir with a high water discharge coefficient is necessary. The ability of a weir to transmit water depends upon the crest length and upstream head. Consequently, by making changes to the geometry (increasing the crest length) in a constant channel width, the carrying capacity increases. For this purpose, labyrinth weirs are more practical than linear weirs, which flow through them more than linear weirs. Today, nonlinear weirs like triangular, trapezoidal, oblique, and parabolic are built in one or more cycles.

Another characteristic of weirs is their ability to dissipate flow energy. The ability to predict this effect enables designers to more accurately calculate changes to flow energy in the system and thus properly design downstream slabs. Most research on labyrinth weirs has focused on their discharge coefficients. However, there is a significant gap in the study of energy loss associated with these types of weirs, highlighting the need for further research and modeling. Additionally, the application of intelligent models to predict energy loss has received limited attention. Energy dissipation is a critical factor in the design of hydraulic structures, especially in weirs, as it directly impacts the downstream flow conditions and the potential for scour or structural damage. In the context of weir design, the primary goal is to ensure that the energy of the flowing water is effectively dissipated to prevent damage to the structure and minimize erosive forces downstream. In weir structures, energy dissipation occurs when the flow transitions from high-velocity supercritical conditions to subcritical conditions, often as a result of flow obstructions such as the weir crest. The amount of energy dissipated is a function of various parameters, including the geometry of the weir, the flow depth, and the velocity of the water. In labyrinth weirs, which are characterized by their non-linear geometry and multi-cycle designs, the energy dissipation process is significantly more complex than in traditional straight-crested weirs.

Hay and Tylor [1] did the first studies on labyrinth weirs. They provided diagrams for the weir design. Tullis et al. [2] investigated trapezoidal plan labyrinth weirs with 6 to 18 apex angles. They described the discharge coefficient (C_d) and its dependence on parameters such as the upstream water level, weir height weir length, and apex angle. Kumar et al. [3] indicated that C_d decreases and length of the interference zone increases as the weir apex angle decreases. Monjezi et al. [4] conducted research on the C_d of arched weirs with a triangular plan form. They concluded that arching weirs increases the efficiency of linear arched weirs and labyrinth arched weirs by up to 21% and 57%, respectivly. Azimi and Hakim [5] studied the rectangular labyrinth weir and showed its suitability for the $h_0/P<0.4$ (h_0 is the head, and P is the weir height). Ayaz and Mansoor [6] analyzed the C_d of labyrinth weirs using ANN model. The results indicated that the ANN successfully predicted the discharge coefficient. The results of Samadi et al. [7] showed that increasing the number of cycles in labyrinth weirs reduces the C_d. Ben Said and Ouamane [8] conducted an experimental and numerical study of rectangular labyrinth weirs. Their results indicated that there is a good agreement between the experimental and numerical results. Also, a weir with a round inlet increases the weir efficiency by 5% compared to a smooth inlet. Zare et al. [9] studied a circular labyrinth weir with various slopes. Their results showed that the highest C_d is for a slope of 60° and the lowest for a state without a slope. Shehata et al. [10] conducted a laboratory study of labyrinth trapezoidal weirs in flow and scour control. Their study indicated that a 60° apex angle provided better results in reducing scour depth and length compared to other angles and a straight weir.

The flow energy dissipation has been investigated in stepped spillways, ogee weirs, chutes, etc. [11-14]. Mohammadzadeh-Habili et al. [15] checked relative energy dissipation (EDR) in labyrinth weirs, resulting that EDR decreases linearly with increasing y_c. Ghaderi et al. [16] conducted a numerical analysis of the C_d and EDR in labyrinth weirs, revealing that C_d values range from 0.4 to 0.8, while EDR varies between 0.6 and 0.3. Furthermore, labyrinth weir structures dissipate between 85% and 70% of flow energy for dimensionless ratios of $1 \geq h_0/P \geq 0.1$ [17]. Furthermore, the research of Idrees and Al-Ameri [18] showed that trapezoidal configurations increase energy

dissipation rates by over 92%. Selim et al. [19] conducted a numerical study of piano key and trapezoidal labyrinth weirs. Their results showed that the energy loss of trapezoidal labyrinth weirs increases with increasing side wall angle. Piano key weirs are preferred over labyrinth trapezoidal weirs at lower ratios ($h_0/P \leq 0.2$), while trapezoidal labyrinth weirs with smaller angles are recommended at higher weir ratios.

While prior studies (e.g., Tullis et al. [2], Kumar et al. [3], Monjezi et al. [4]) have extensively explored discharge coefficients (C_d) in labyrinth weirs, they often overlook the critical aspect of energy dissipation. Only a few studies, such as Haghiabi et al. [17], specifically address EDR, and even these are limited to specific weir configurations and flow conditions. Most prior research relies on empirical equations or experimental analysis for modeling hydraulic performance. Although these approaches provide valuable insights, they lack the generalizability and predictive accuracy required for diverse real-world applications. Existing studies primarily focus on a narrow range of weir geometries (e.g., trapezoidal and triangular forms). However, the influence of different cycle types and configurations on energy dissipation has not been systematically evaluated. For instance, research by Selim et al. [19] and Idrees and Al-Ameri [18] briefly mentions geometric impacts but lacks detailed modeling of their effects on EDR.

Several key hydraulic phenomena contribute to energy dissipation in labyrinth weirs:

Flow Contraction and Expansion: As water approaches the labyrinth weir, it is first subjected to flow contraction, which increases the flow velocity. Upon crossing the weir crest, the flow expands rapidly. These sudden changes in flow direction and velocity lead to the formation of turbulent zones, which are the primary contributors to energy loss.

Flow Separation and Reattachment: The unique geometry of labyrinth weirs, such as the triangular or trapezoidal cycle shapes, induces flow separation at the crest of each cycle. As the flow separates, vortexes and turbulent eddies are generated. These vortices and their subsequent reattachment downstream create localized energy dissipation zones, enhancing the overall energy loss in the system. This phenomenon is particularly prominent in multi-cycle labyrinth weirs.

Hydraulic Jump: For larger flow discharges, the flow may become supercritical (high velocity) as it flows over the crest of the weir. When this supercritical flow transitions to subcritical flow downstream, a hydraulic jump is formed. During the hydraulic jump, a significant portion of the flow's kinetic energy is converted into turbulent energy, resulting in substantial energy dissipation. In labyrinth weirs, the multiple cycles often promote the formation of such jumps at various locations, further increasing the energy dissipation.

Turbulent Flow in Weir Cycles: In labyrinth weirs, the multi-cycle design creates a series of bends and turns for the flow. These changes in direction cause the flow to become turbulent, with vortices and eddies dissipating kinetic energy. The turbulence is particularly strong in the regions between the weir cycles, where the flow interacts with the weir surface and the channel bed.

Cavitation and Flow Impingement: In some cases, the flow may impinge on the weir surface, generating localized areas of high shear stress and turbulence. This can lead to the formation of cavitation bubbles, which contribute to further energy loss. Although cavitation is not always a significant factor in labyrinth weirs, it can become relevant under high flow conditions.

The discussion of these hydraulic phenomena lays the foundation for understanding the energy dissipation process in labyrinth weirs. By considering these phenomena, we can better appreciate how the geometry and flow characteristics of a labyrinth weir influence the efficiency

of energy dissipation. This understanding provides the necessary context for exploring advanced computational models, such as those based on machine learning, to predict energy dissipation more accurately. The complexity of the flow and energy dissipation process in labyrinth weirs, therefore, necessitates the development of robust predictive models that account for the dynamic and non-linear nature of these systems.

A considerable number of previous studies have focused on investigating the flow rate of labyrinth weirs. The research on the labyrinth weir's energy dissipation has been done in a limited way, and except for a few researches, it has not been carried out yet widely. Given the inherent uncertainties surrounding energy dissipation modeling in previous studies, further investigation into intelligent modeling approaches for energy dissipation in labyrinth weirs with varying plan forms appears essential. Accordingly, this study focuses on analyzing the energy dissipation in labyrinth weirs with triangular and trapezoidal configurations across various cycle types. Using experimental data, the performance of intelligent modeling techniques-including ANN, SVM, and RF algorithm−has been evaluated in predicting energy dissipation.

2. Materials and Methods

Here, the data of Haghiabi et al. [17] have been used. Triangular and trapezoidal plan labyrinth weirs with single and double cycles were used. The EDR in the labyrinth weir is calculated according to Equation (1) [15,17].

$$E_0 = y_0 + \frac{q^2}{2gy_0^2}$$
$$E_1 = y_1 + \frac{q^2}{2gy_1^2} \quad (1)$$
$$EDR = \frac{\Delta E}{E_0} = \frac{E_0 - E_1}{E_0}$$

In the above equations, E_0 and E_1 represent the specific energy of the flow (L), y_0 and y_1 represent the flow depth (L), q is the flow rate per unit width of the channel (L^2T^{-1}), g is the gravitational acceleration (LT^{-2}), and ΔE is the energy dissipation (L).

According to Haghiabi et al. [17] and Equation (2), the most significant parameters affecting EDR are:

$$EDR = f_1(W_c, W_{cy}, L_{cy}, L_{cr}, P, V_0, h_0, g, \rho) \quad (2)$$

In Equation (2), h_0 represents the flow depth above the weir (L), V_0 is the velocity (LT^{-1}), g is the gravitational acceleration (LT^{-2}), P represents the weir height (L), ρ is the specific gravity of water (ML^{-3}), W_c is the channel width (L), W_{cy} is the width of one weir cycle (L), L_{cy} is the length of one weir cycle (L), L_{cr} total length of the crest (L). According to Haghiabi et al. [17] and Buckingham theorem as dimensional analysis technique and by considering the V_0, g and ρ as repetitive parameter, the non-dimensional parameters are derived as Equation (3). Since the flow upstream of the weir is subcritical, the effect of the Froude number can be ignored. The Reynolds number can also be neglected due to the turbulence of the flow. Figure (1) indicates the picture of the triangular and trapezoidal plan labyrinth weir.

$$EDR = f_2\left(\frac{h_0}{P}, \frac{W_c}{W_{cy}}, \frac{L_{cy}}{W_{cy}}\right) \quad (3)$$

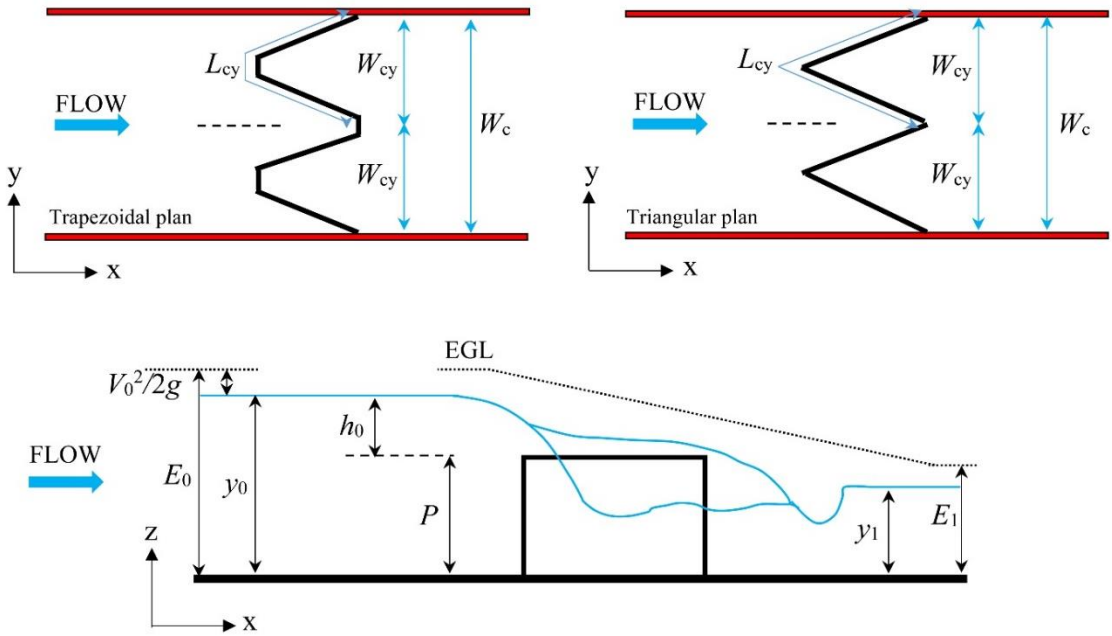

Figure 1. View of the labyrinth weir [17]

2.1. Support Vector Machine (SVM)

SVM is a supervised learning model widely applied for both classification and prediction tasks [20]. The algorithm employs constrained optimization to minimize structural penalty, thereby achieving an optimal response. It functions by estimating a model that associates the dependent variable with several independent input parameters [21,22]. The function can be written as Equation (4):

$$f(x) = \sum_{i=1}^{N} \bar{a}_i \emptyset(X_i)^T \emptyset(X) + b \qquad (4)$$

The a_i represents the mean Lagrange coefficients. Calculating ø(X) can be very complicated. The SVM regression uses a kernel function that depends on the size of the training data and the dimensions of the feature vector. In practice, four types of Lin. kernel, Poly. kernel, Sig. kernel, and Radial Basis Function kernel (RBF) are used.

$$K(X_i, X_j) = (X_i, X_j) \qquad (5)$$

$$K(X_i, X_j) = \left(1 + (X_i, X_j)\right)^d \qquad (6)$$

$$K(X_i, X_j) = tanh\left(-a(X_i, X_j) + C\right) \qquad (7)$$

$$K(X_i, X_j) = exp(-\|X - X_i\|^2/\sigma^2) \qquad (8)$$

2.2. Artificial Neural Network (ANN)

ANN comprises input layers, hidden layers, and output layers that collectively facilitate decision-making processes. Within this structure, neurons serve as fundamental units that transform input signals before transmitting processed information to subsequent layers. The architecture of the network consists of interconnected mathematical operations, often nonlinear, that enable complex interactions across layers, resulting in sophisticated and nonlinear behaviors. Although each neuron functions independently, the network as a whole demonstrates cohesive behavior. While ANNs share certain similarities with human neural activity, there are notable differences in terms of training processes, operational behavior, and computational capacity [23].

2.3. Random Forest algorithm (RF)

RF is a supervised learning model that typically leverages the bagging method, which combines multiple learning models to enhance overall performance. In RF, multiple decision trees are constructed and

merged, resulting in superior predictive accuracy [24]. Random forests are applicable to both classification and regression tasks. During the training or model-fitting phase, the RF model maps input data to outputs by learning from data relevant to the target problem domain. Through this process, the model identifies and learns underlying relationships within the data to accurately predict the desired output values [25].

2.4. Statistical indicators

Here, the following statistical indicators were employed [26-28]:

$$RE\% = \frac{X_{Obs} - X_{cal}}{X_{Obs}} \times 100 \quad (9)$$

$$RMSE = \sqrt{\frac{\sum_{i=1}^{n}(X_{Obs} - X_{Cal})_i^2}{n}} \quad (10)$$

$$KGE = 1 - \sqrt{(R-1)^2 + (\beta-1)^2 + (\gamma-1)^2}$$
$$\beta = \frac{\overline{X_{Cal}}}{\overline{X_{Obs}}}, \gamma = \frac{CV_{Cal}}{CV_{Obs}}$$
$$R = \frac{[\sum_{i=1}^{n}(X_{Obs\,i} - \overline{X_{Obs}}) \times (X_{Cal\,i} - \overline{X_{Cal}})]}{\sum_{i=1}^{n}(X_{Obs\,i} - \overline{X_{Obs}}) \sum_{i=1}^{n}(X_{Cal\,i} - \overline{X_{Cal}})} \quad (11)$$

Here, Equation (9 to11) represent the percentage relative error, root mean square error, and King Gupta Efficiency, respectively. Also, in Equation (12), R, β and γ represent the coefficient of correlation, ratio of the mean cal to the mean obs and ratio of the standard deviation of cal to the standard deviation of the observed, respectively.

3. Results and Discussion

The objective was to assess the applicability of modern data mining techniques for estimating EDR. A dataset comprising 70% of the data was allocated for the training phase, and the remaining 30% for testing.

As indicated in Table (1), among the Lin., Poly., RBF, and Sig. kernels, the RBF was identified as the optimal choice for the SVM. The comparison among obs and cal values of EDR is illustrated in Figures (2a and b) for various kernels. Additionally, various data sets are depicted in Figure (2c). The RBF demonstrated significantly higher accuracy compared to the other kernels, effectively predicting EDR with notable precision.

Figures (2d and e) present the statistical performance indicators for the RBF during the training phase, with values of 0.952, 0.0076, 0.0078 and 0.865 for R, RMSE, Mean RE, and KGE, respectively. For the testing phase, the corresponding values were 0.907, 0.0153, 0.0138, and 0.744, respectively. Figures (2f and g) further illustrate that the superior kernel maintains a wide range of data points within the $\pm$3% RE band. Specifically, in the training phase, 100% of the data points fall within this error band, while 96% of the data points in the testing phase also fall within the same margin.

Table 1. The results of the test statistical indices of various kernels in the SVM

Indicators	Lin.	Poly.	RBF	Sig.
Coefficient of correlation	0.530	0.239	0.907	0.292
Kling Gupta Efficiency	0.308	0.007	0.744	-0.912
Root Mean Square Error	0.0319	0.0359	0.0153	0.0992
Mean Relative Error %	3.150	2.937	1.38	8.564

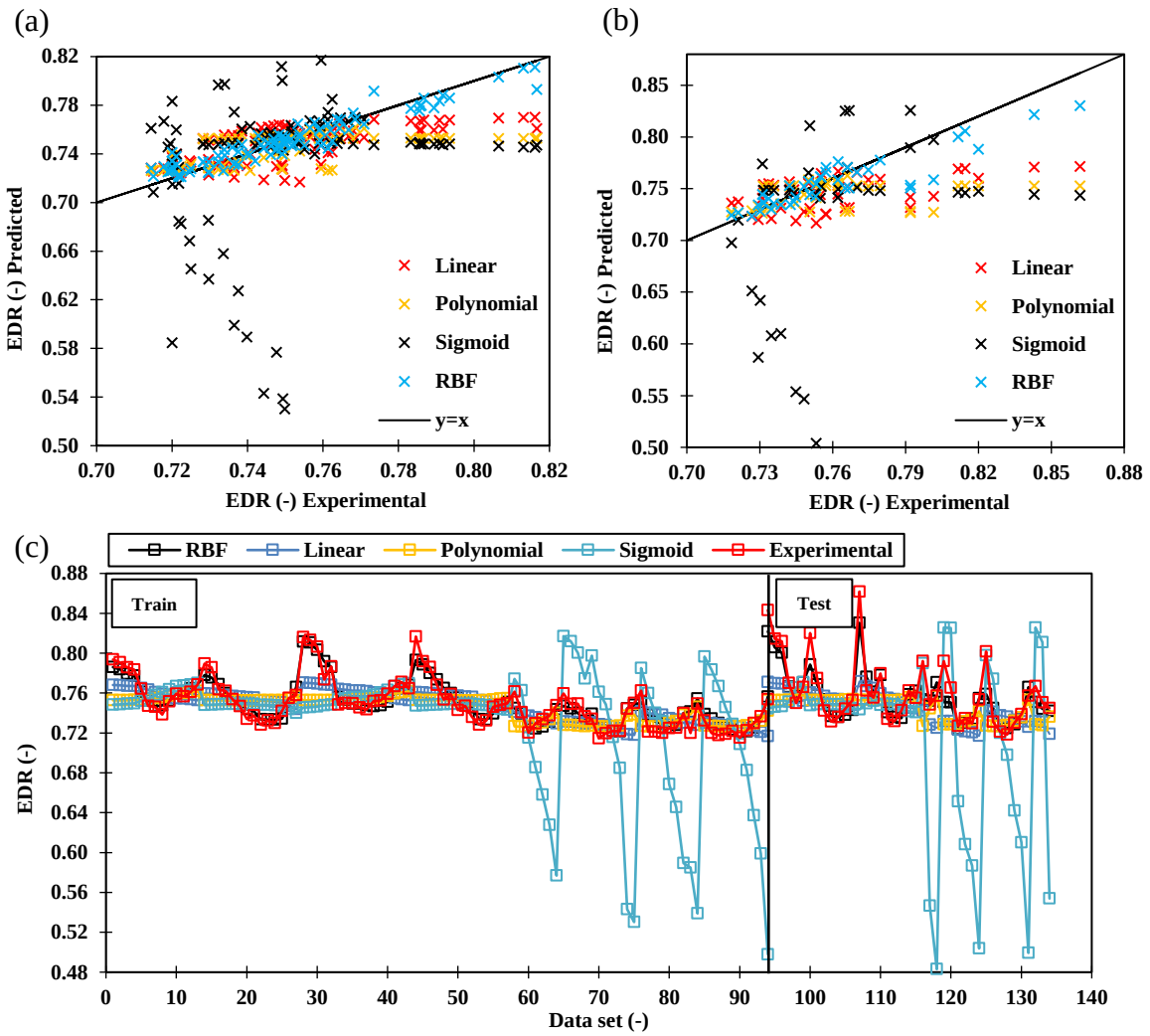

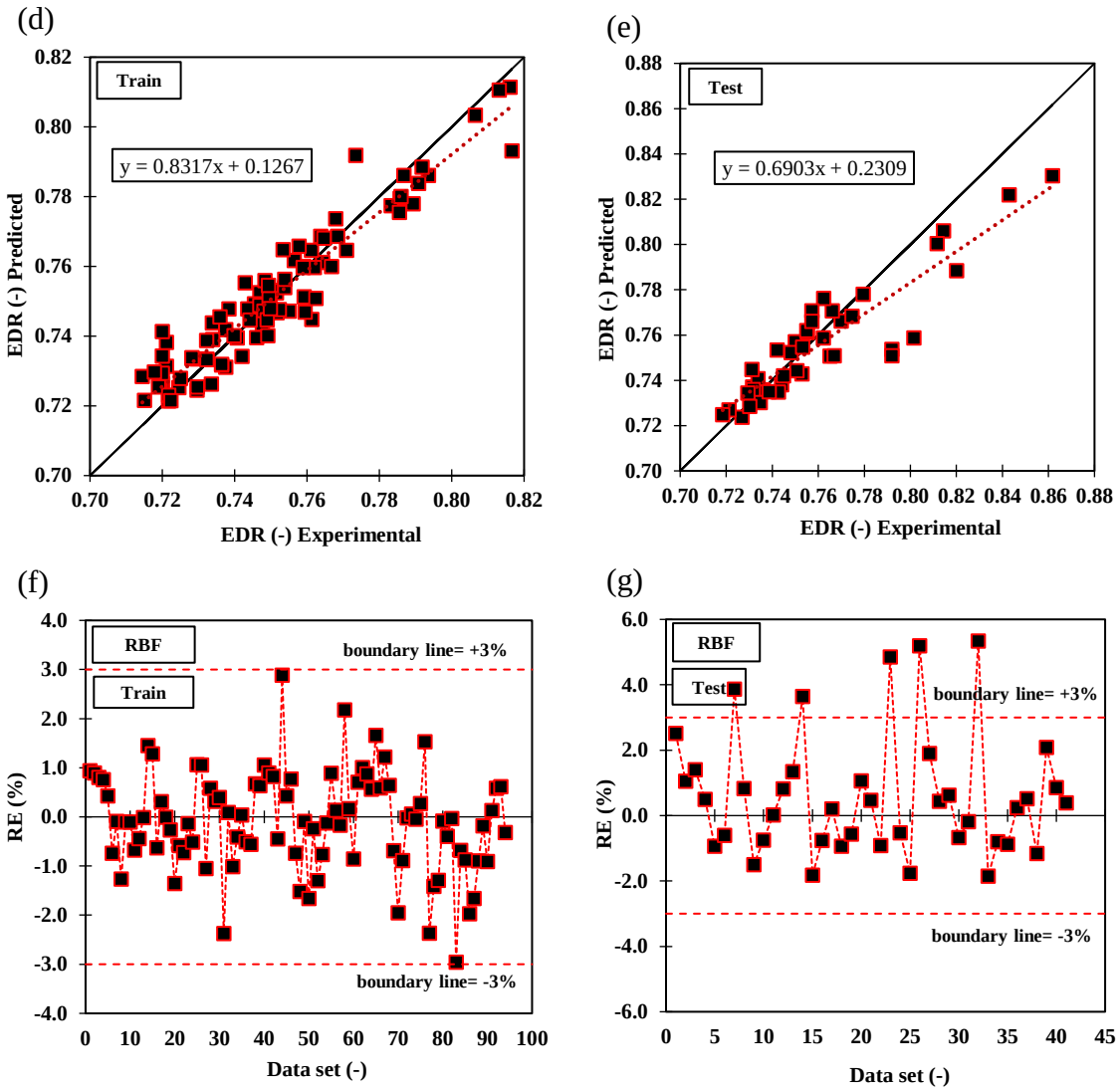

Figure 2. Experimental versus predicted values

In the ANN method, similar to the SVM model, 70% of the data were randomly allocated for training, while the remaining 30% were designated for testing, facilitated by the software. As depicted in Figure (3), the accuracy of the multilayer perceptron (MLP) network improved in comparison to the radial basis function (RBF) network. For the MLP network, the performance metrics of R, RMSE, Mean RE and KGE were 0.972, 0.0064, 0.64%, and 0.958, respectively (training phase). In the testing phase, the statistical metrics were 0.969, 0.0070, 0.73%, and 0.968, respectively.

In contrast, the RBF network yielded training phase results of 0.871, 0.0134, 1.16% and 0.815 for R, RMSE, Mean RE and KGE, respectively. During the testing phase, the corresponding values were 0.943, 0.103, 1.04% and 0.941, respectively. In the test phase, the MLP and RBF networks exhibited data within the ±2.80% and ± 10.3% RE ranges, respectively. Consequently, based on these results, the MLP method was identified as the superior model at this stage.

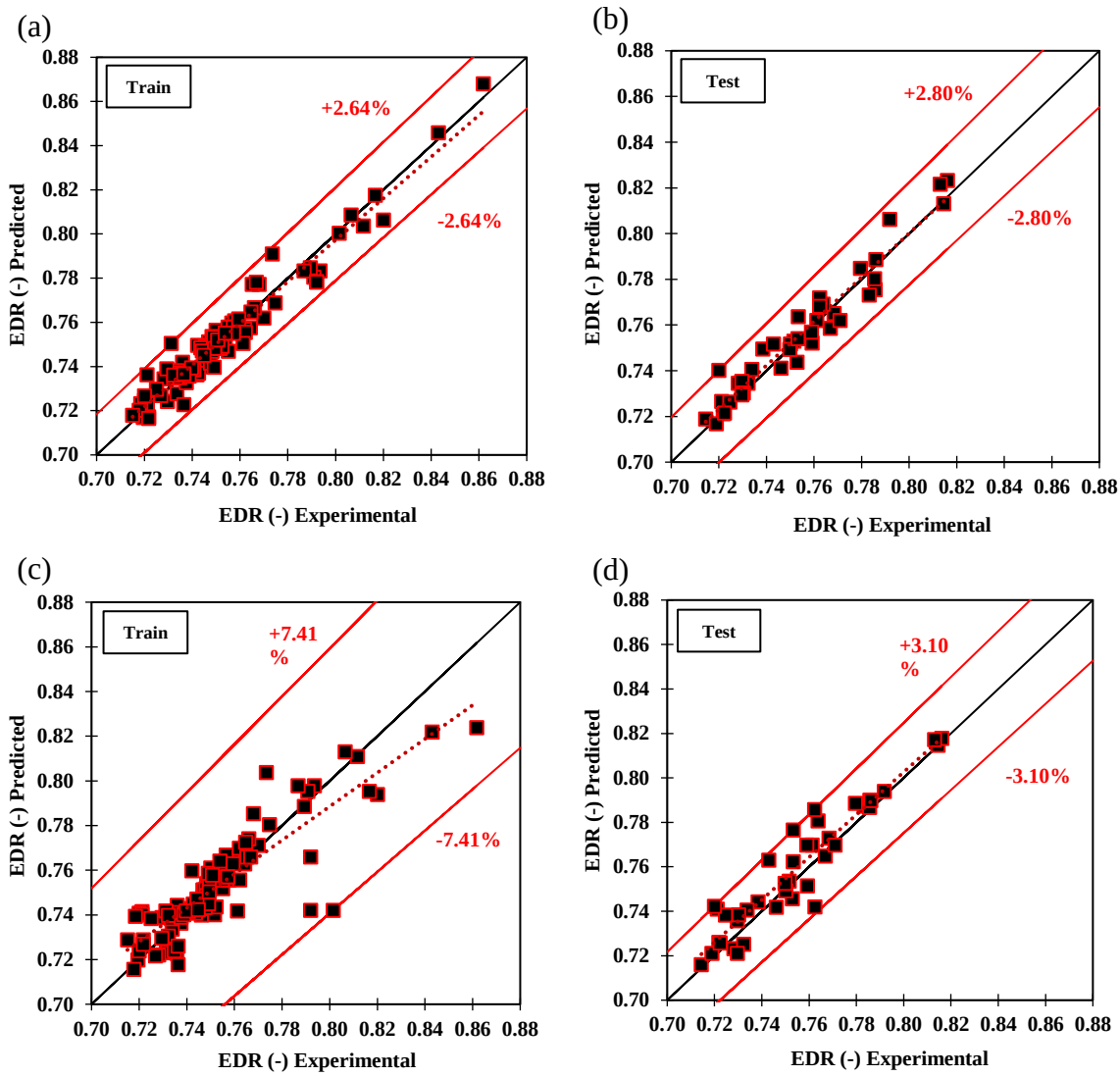

Figure 3. Experimental values versus predicted, a and b) MLP, c and d) RBF

Figures (4a and c) show the scatter diagram of the data in the training and test phase for the RF model. Here, R=0.878, RMSE=0.0188, Mean RE%=1.78% and KGE=0.362 for the training phase. For the test stage, it is equal to 0.898, 0.0193, 1.91%, and 0.369, respectively. Although the value of the Mean RE in the RF model in the training and test phase are 1.78% and 1.91%, respectively, it is not possible to make a decision based on the result of this index. The reason for these values can be pointed to close observed data so that the EDR is in the range of 0.714 to 0.862. Therefore, these results are not good. The KGE for this model is less than 0.4 and it is in the unsatisfactory part, which indicates the lack of proper ability of this model in predicting the amount of EDR. Figures (4b and d) show the overlap of the experimental and predicted data for different data in the training and test phase, which are significantly different from each other. The detailed discussion of the potential reasons of low statistical indexes are as follows:

1. Sensitivity to Data Characteristics: The RF model aggregates predictions from multiple decision trees, which makes it robust to noise but less capable of

capturing subtle nonlinear interactions in data. Since energy dissipation in labyrinth weirs involves complex, nonlinear relationships between hydraulic and geometric parameters, RF may have struggled to adequately capture these complexities.

2. Limited Variability in Experimental Data: The experimental dataset used in this study, while well-structured, covers a relatively narrow range of flow conditions and geometric configurations. This limited variability can reduce the effectiveness of RF, as its ensemble approach relies on diverse data splits to construct highly predictive trees.
3. KGE's Sensitivity to Model Bias: The low KGE observed for the RF model may stem from its tendency to underestimate or overestimate specific ranges of energy dissipation. Since KGE accounts for correlation, bias, and variability, even small biases in RF predictions can lead to a lower overall score compared to metrics like RMSE or mean relative error (RE%).
4. Overfitting to Training Data: Although RF generally reduces overfitting compared to individual decision trees, it can still overfit if the number of trees is too high or the maximum depth of trees is not restricted. Overfitting could have reduced the model's ability to generalize to the testing dataset, thereby affecting its performance.

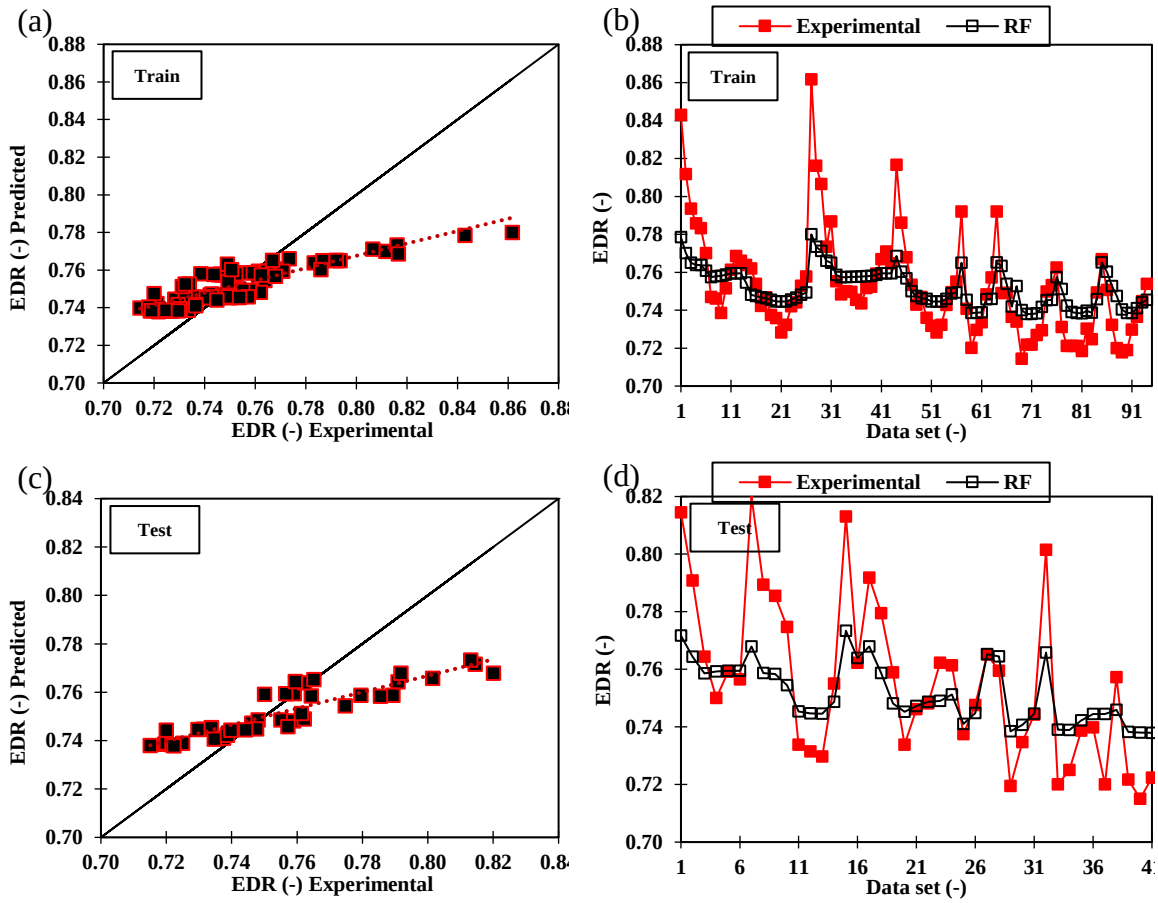

Figure 4. Experimental values versus predicted in RF model

Figure (5) presents the optimal outcomes for each model group−SVM, ANN, and RF −to determine the most effective approach for predicting EDR. As illustrated in Figure (5a), the RF model's predictions fall within a RE range of ±9.36%, with an RMSE and Mean RE% of 0.0193 and 1.91%, respectively. In contrast, the SVM model using the RBF kernel demonstrated improved accuracy over the RF model, yielding data within a RE range of ±5.34% and achieving an RMSE of 0.0153 and a Mean RE% of 1.38%. Among the models, the ANN-MLP method exhibited the most accurate performance, with results closely aligned with experimental data. For the ANN-MLP model, predictions fell within a ±2.80% RE range, with RMSE and Mean RE% values of 0.0070 and 0.73%, respectively. The correlation coefficients for the RF, SVM-RBF, and ANN-MLP models in the test phase were 0.898, 0.907, and 0.969, respectively. A comparative analysis of EDR predictions and experimental data indicates a superior alignment of ANN model outputs with experimental results, as shown in Figure (5b). The superior performance of the ANN can be attributed to several key factors, which are discussed below:

1- Ability to Capture Nonlinear Relationships: The ANN, specifically the Multilayer Perceptron (MLP) architecture used in this study, is inherently well-suited for modeling complex and nonlinear relationships in datasets. Energy dissipation in labyrinth weirs is influenced by multiple interacting parameters, such as flow depth, weir height, and cycle geometry, which exhibit nonlinear dependencies. The ANN's capability to model these interactions more effectively than the SVM and RF algorithms likely contributed to its superior predictive accuracy.

2- Data Characteristics: The dataset used in this study comprises well-structured experimental data with consistent trends and relationships, which ANN models can leverage effectively. The network's ability to adjust weights and biases during training allows it to identify and exploit patterns in the data that may not be as easily captured by other models.

3- Flexible Model Architecture: The architecture of the MLP used in this study, with multiple hidden layers and nonlinear activation functions, provides greater flexibility in learning intricate relationships between input and output variables. This flexibility may explain why the ANN outperformed SVM, which relies on kernel functions, and RF, which aggregates multiple decision trees but may not handle complex nonlinearities as efficiently.

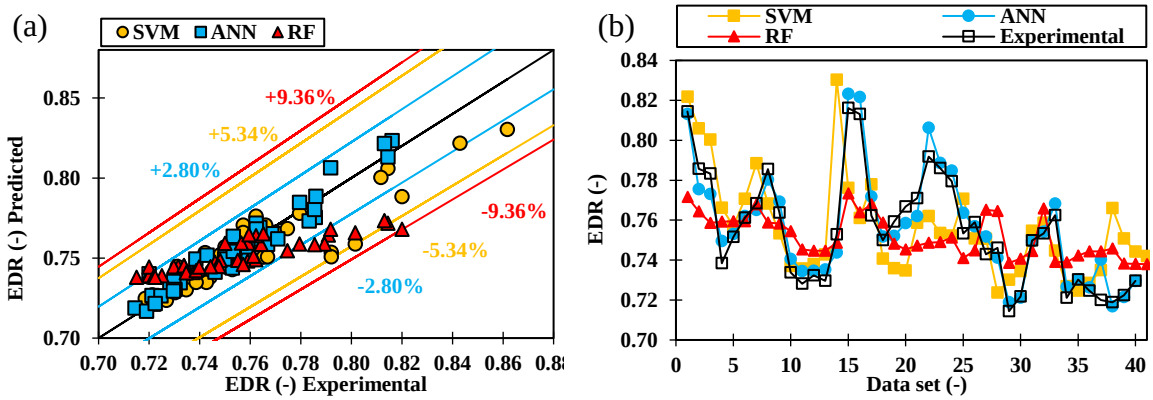

Figure 5. Experimental values versus predicted for different models in the test phase

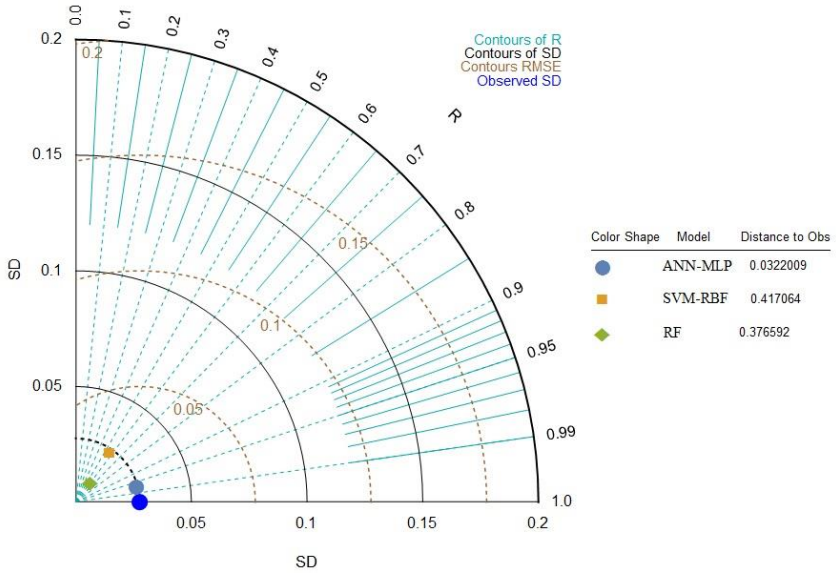

Figure 6. Taylor diagram

The Taylor diagram confirms that the ANN-MLP model significantly outperforms the SVM-RBF and RF models in predicting the EDR for labyrinth weirs (Figure 6). Its high correlation coefficient, low RMSE, and accurate standard deviation matching make it the most robust and reliable model [27]. These findings highlight the ANN model's The high EDR of labyrinth weirs can be attributed to the following main processes:

1. The collision of the flow near the upstream vortices and between the triangular and trapezoidal weir cycles. According to the research of Crookston and Tullis [29] and Mohammadzadeh-Habili et al. [15], the flow impinging on the weir creates a local hydraulic jump condition near the upstream vortices, which leads to energy dissipation.
2. The turbulent flow creates a pool in front of the weir. In a labyrinth weir, the return flow caused by the impact of the flow falling with the channel bed leads to the formation of an eddy flow in the pool behind the flow jet (in front of the weir). The pool flow energy is dissipated through turbulent eddies.
3. Supercritical flow collides at the channel base and a hydraulic jump is formed downstream of the weir. During the hydraulic jump, a significant part of the energy is lost. As the discharge increases, the performance of labyrinth weirs decreases. The main reason for this is that the flow fills the space among the weir cycles. By increasing the discharge, the opportunity to drain the flow from the space among the cycles is lost. The highest value of EDR is related to single-cycle weirs. As L_{cy}/W_{cy} increases, the flow energy dissipation decreases. At $h_0/P \geq 0.5$, this amount goes through the same process. In addition, the reason why the trapezoidal plan weir inferior to triangular plan weir for energy dissipation. This observation is related to the reduction of head dissipation due to the sudden change of the inlet and outlet streamlines [17].

potential as a powerful tool for hydraulic engineering applications, particularly in modeling energy dissipation in complex flow systems. This analysis strengthens the conclusion that ANN is the preferred model for accurate and reliable predictions, making it a valuable contribution to the design and optimization of labyrinth weirs.

In this research, by using Solver in Excel software, relationships have been presented to predict the amount of energy dissipation of labyrinth weirs with triangular and trapezoidal plans, respectively, within the scope of this research:

$$EDR = -5.10\left(\frac{h_0}{p}\right)^{0.004} + 1.30\left(\frac{L_{cy}}{W_{cy}}\right)^{-0.044} + 4.58\left(\frac{W_c}{W_{cy}}\right)^{0.0045} \quad (12)$$

$$EDR = -1.72\left(\frac{h_0}{p}\right)^{0.012} + 0.094\left(\frac{L_{cy}}{W_{cy}}\right)^{-0.825} + 2.418\left(\frac{W_c}{W_{cy}}\right)^{0.004} \quad (13)$$

The results of Mean RE% for the above relationships are 1.86% and 2.12%, respectively. The amount of RMSE are 0.017, and 0.019, respectively. For the relationships, KGE is in the very good range. The results showed that the above relationships have high accuracy in predicting energy dissipation, so for the above relationships, more than 82% and 83% of the data are within the RE range of ±3%, respectively.

The comparison of the statistical metrics for derived equations with those from the previous studies shows the following:

Table 2. The results of the present study with previous studies

Study	RMSE (-)	Mean RE (%)	KGE (-)
Equation (12)	0.017	1.86	0.96
Equation (13)	0.019	2.12	0.94
Mohammadzadeh-Habili et al. [15]	0.021	2.02	0.91
Haghiabi et al. [17]	0.023	2.14	0.89

The derived equations for predicting EDR in labyrinth weirs show superior performance when compared to previous studies. The statistical results, including RMSE, Mean RE%, and KGE, confirm the enhanced accuracy and robustness of these models. The new equations are more reliable and applicable to a wider range of weir configurations, making them a valuable tool for predicting energy dissipation in labyrinth weir design and analysis.

To strengthen the analysis of the derived equations and their relevance to hydraulic principles, we have incorporated a discussion that relates the empirical formulas for energy dissipation rate with established hydraulic concepts. This analysis aims to validate the theoretical underpinnings of the equations and demonstrate their physical relevance in the context of labyrinth weirs.

Hydraulic Evidence for EDR Equations

Energy dissipation in weir structures, particularly labyrinth weirs, is primarily governed by the following hydraulic phenomena:

1. Flow Contraction and Expansion: As water flows over the labyrinth weir, it undergoes contraction at the entrance and expansion at the outlet. These transitions induce turbulence, which is a significant factor contributing to energy loss.

2. Flow Separation and Reattachment: The non-linear geometry of labyrinth weirs, with their multi-cycle configuration, causes complex flow patterns. Flow separation near the weir's crest and the subsequent reattachment downstream creates vortices, which enhance the energy dissipation.

3. Hydraulic Jump: In cases of high discharge, supercritical flow on the weir face may transform into subcritical flow downstream, forming a hydraulic jump. This phenomenon is a major contributor to energy dissipation.

4. Turbulent Flow in the Weir Cycles: The multiple cycles of a labyrinth weir create additional surfaces where water can interact with the channel bed, inducing turbulent flow that contributes to energy loss. This is particularly evident in the formation of eddies and vortices in front of and behind the weir cycles.

The derived equations for EDR incorporate these hydraulic principles through their dependence on key geometrical and flow parameters, such as:
$\boldsymbol{h_0}$: The flow depth above the weir, which influences the potential energy available for dissipation.
$\boldsymbol{P}$: The weir height, which directly affects the flow velocity and, thus, the kinetic energy dissipated.
$\boldsymbol{W_c}$ and $\boldsymbol{W_{cy}}$: These parameters describe the width of the channel and the weir cycles, which control the flow interactions and turbulence intensity.
$\boldsymbol{L_{cy}}$: The length of one weir cycle, which impacts the flow path and the degree of energy dissipation through the turbulence and vortices.

Physical Interpretation of Derived Equations

We can now analyze the physical behavior predicted by the derived equations using hydraulic principles:
The Equations indicate a strong dependence on h_0, P, and W_{cy}. These findings align with established hydraulic theory, where the flow depth (h_0) and weir height (P) are key drivers of flow velocity and energy conversion, respectively.
The presence of W_{cy} and L_{cy} in the equations is consistent with the idea that the geometry of the weir affects the flow dynamics. Wider and longer weir cycles (W_{cy} and L_{cy}) tend to induce more complex flow patterns, including turbulence and vortices, which enhance energy dissipation.
The lower Mean Relative Error (RE%) and Root Mean Square Error (RMSE) values observed for the derived equations suggest that these parameters are effectively capturing the physical processes of energy dissipation. This is consistent with the hydraulic understanding that energy loss is most prominent where flow separation, turbulence, and hydraulic jumps occur, particularly in non-linear weir geometries like those in labyrinth weirs.
By analyzing the derived equations through the lens of hydraulic principles, we demonstrate that the empirical formulas for predicting EDR are not only statistically robust but also consistent with established hydraulic theory. The dependence of the equations on flow depth, weir height, and cycle geometry supports their physical relevance and underscores their ability to model the complex flow phenomena involved in energy dissipation in labyrinth weirs.

4. Conclusions

In this study, data mining techniques−support vector machine (SVM), artificial neural network (ANN), and random forest (RF)−were employed to predict energy dissipation in labyrinth weirs. The primary objective was to assess the predictive accuracy of these methods and identify the most effective approach for modeling this complex hydraulic phenomenon. Each model utilized a dataset split, with 70% of the data allocated for training and 30% for testing. The results revealed several significant findings, limitations, and opportunities for further research, which are detailed below.

Key Findings:

Support Vector Machine (SVM):
The SVM model's performance was critically analyzed using various kernel functions, including polynomial, linear, sigmoid, and radial basis function (RBF). Among these, the RBF kernel demonstrated superior predictive accuracy. The performance metrics for the SVM-RBF model in the testing phase included a coefficient of determination (R) of 0.907, a root mean square error (RMSE) of 0.0153, a mean relative error percentage (Mean RE%) of 1.38%, and a Kling-Gupta efficiency (KGE) of 0.744. These metrics underscore the RBF kernel's ability to closely align with experimental results, making it a robust choice for this application.
Artificial Neural Network (ANN):
The ANN approach explored two types of networks: multilayer perceptron (MLP) and radial basis function (RBF). The MLP

network outperformed the RBF network in terms of predictive accuracy. By leveraging its capacity to model complex non-linear relationships, the MLP network emerged as the most effective among all models tested in this study. This finding highlights the potential of ANN, particularly the MLP structure, in modeling energy dissipation phenomena with high precision.

Random Forest (RF):

While the RF model exhibited acceptable predictive capabilities, its performance was inferior compared to the SVM-RBF and ANN-MLP models. This result aligns with the understanding that ensemble-based models like RF, while robust, may not capture the intricate non-linear relationships in hydraulic systems as effectively as ANN and SVM models.

Non-Linear Polynomial Regression Equations:

In addition to data mining models, non-linear polynomial regression equations were developed to enhance predictive modeling. These equations provided supplementary insights into the relationship between the input variables and energy dissipation, offering a simpler yet less accurate alternative compared to the machine learning models.

Limitations:

Dataset Size and Diversity:

The dataset used in this study was limited in size and scope, which may impact the generalizability of the findings. Future studies should consider larger and more diverse datasets to validate the robustness of the models across different conditions and geometries.

Unconsidered Variables:

The study focused on a specific set of input variables to predict energy dissipation. However, other potentially influential factors, such as flow turbulence characteristics and material properties, were not included. Incorporating these factors in future models could enhance predictive accuracy.

Model Complexity:

While the ANN and SVM models demonstrated high accuracy, their computational complexity might limit their practical application in scenarios requiring real-time predictions. Simplifying these models without compromising accuracy could improve their utility in field applications.

Recommendations for Future Research:

Building upon the findings and limitations of this study, several recommendations for future research are proposed:

Dataset Expansion:

Future studies should prioritize collecting and incorporating larger, more diverse datasets from different labyrinth weir configurations, flow conditions, and experimental setups. This will ensure broader applicability of the models and enhance their generalizability.

Exploration of Advanced Techniques:

While this study focused on SVM, ANN, and RF models, emerging machine learning techniques, such as deep learning, gradient boosting algorithms, and hybrid models, could be explored. These methods may offer improved performance and new insights into the predictive modeling of energy dissipation.

In summary, this study demonstrates the potential of data mining techniques, particularly SVM and ANN, in accurately predicting energy dissipation in labyrinth weirs. Among the models tested, the ANN-MLP model emerged as the most effective, followed closely by the SVM-RBF model. These findings contribute to the growing body of knowledge on the application of machine learning in hydraulic engineering, offering new avenues for optimizing the design and performance of hydraulic structures.

References

1. Hay, N., & Taylor, G. (1970). Performance and design of labyrinth weirs. Journal of the Hydraulics Division, 96(11), 2337-2357.
2. Tullis, B. P., Young, J. C., & Chandler, M. A. (2007). Head-discharge relationships for submerged labyrinth weirs. Journal of hydraulic engineering, 133(3), 248-254.
3. Kumar, S., Ahmad, Z., & Mansoor, T. (2011). A new approach to improve the discharging capacity of sharp-crested triangular plan form weirs. Flow measurement and instrumentation, 22(3), 175-180.
4. Monjezi, R., Heidarnejad, M., Masjedi, A., Purmohammadi, M. H., & Kamanbedast, A. (2018). Laboratory investigation of the Discharge Coefficient of flow in arced labyrinth weirs with triangular plans. Flow Measurement and Instrumentation, 64, 64-70.
5. Azimi, A. H., & Hakim, S. S. (2019). Hydraulics of flow over rectangular labyrinth weirs. Irrigation Science, 37(2), 183-193.
6. Ayaz, M., & Mansoor, T. (2021). Development of ANN model for discharge prediction and optimal design of sharp-crested triangular plan form weir for maximum discharge using linked ANN–optimization model. Water Supply, 21(6), 3027-3041.
7. Samadi, A., Salmasi, F., Arvanaghi, H., & Mousaviraad, M. (2022). Effects of geometrical parameters on labyrinth weir hydraulics. Journal of Irrigation and Drainage Engineering, 148(10), 06022006.
8. Ben Said, M., & Ouamane, A. (2022). Performance of rectangular labyrinth weir–an experimental and numerical study. Water Supply, 22(4), 3628-3644.
9. Zare, H., Vaghefi, M., Mahmoudi, A., & Behroozi, A. M. (2023). Experimental exploration of flow hydraulics and discharge coefficient for an inclined circular labyrinth weir. Water Resources Management, 37(11), 4521-4536.
10. Shehata, A. H., Youssef, T. F., Hamada, H. A., & Samy, A. (2024). Optimizing Trapezoidal Labyrinth Weir Design for Enhanced Scour Mitigation in Straight Channels. Water, 16(17), 2443.
11. Parsaie, A., & Haghiabi, A. H. (2019). The hydraulic investigation of circular crested stepped spillway. Flow Measurement and Instrumentation, 70, 101624.
12. Zhou, Y., Wu, J., Ma, F., & Qian, S. (2021). Experimental investigation of the hydraulic performance of a hydraulic-jump-stepped spillway. KSCE Journal of Civil Engineering, 25, 3758-3765.
13. Biabani, R., Salmasi, F., Nouri, M., & Abraham, J. (2022). Flow over embankment gabion weirs in free flow conditions. Journal of Hydro-Environment Research, 44, 65-76.
14. Salmasi, F., & Abraham, J. (2023). Hydraulic characteristics of flow over stepped and chute spillways (case study: Zirdan Dam). Water Supply, 23(2), 851-866.
15. Mohammadzadeh-Habili, J., Heidarpour, M., & Samiee, S. (2018). Study of energy dissipation and downstream flow regime of labyrinth weirs. Iranian Journal of Science and Technology, Transactions of Civil Engineering, 42, 111-119.
16. Ghaderi, A., Daneshfaraz, R., Dasineh, M., & Di Francesco, S. (2020). Energy dissipation and hydraulics of flow over trapezoidal–triangular labyrinth weirs. Water 12 (7): 1992.
17. Haghiabi, A. H., Nou, M. R. G., & Parsaie, A. (2022). The energy dissipation of flow over the labyrinth weirs. Alexandria Engineering Journal, 61(5), 3729-3733.
18. Idrees, A. K., & Al-Ameri, R. (2023). Investigation of flow characteristics and energy dissipation over new shape of the trapezoidal labyrinth weirs. Flow Measurement and Instrumentation, 89, 102276.
19. Selim, T., Hamed, A. K., Elkiki, M., & Eltarabily, M. G. (2024). Numerical

investigation of flow characteristics and energy dissipation over piano key and trapezoidal labyrinth weirs under free-flow conditions. Modeling Earth Systems and Environment, 10(1), 1253-1272.
20. Vapnik VN (1995) The nature of statistical learning theory. Springer-Verlag, New York
21. Daneshfaraz, R., Santos, C. A. G., Norouzi, R., Kashani, M. H., AmirRahmani, M., & Band, S. S. (2023). Prediction of drop relative energy dissipation based on Harris Hawks Optimization algorithm. Iranian Journal Of Science And Technology, Transactions Of Civil Engineering, 47(2), 1197-1210.
22. Norouzi, R., Sihag, P., Daneshfaraz, R., Abraham, J., & Hasannia, V. (2021). Predicting relative energy dissipation for vertical drops equipped with a horizontal screen using soft computing techniques. Water Supply, 21(8), 4493-4513.
23. Al-Bulushi, N. I., King, P. R., Blunt, M. J., & Kraaijveld, M. (2012). Artificial neural networks workflow and its application in the petroleum industry. Neural Computing and Applications, 21, 409-421.
24. Sun, D., Lonbani, M., Askarian, B., Jahed Armaghani, D., Tarinejad, R., Thai Pham, B., & Huynh, V. V. (2020). Investigating the applications of machine learning techniques to predict the rock brittleness index. Applied Sciences, 10(5), 1691.
25. Jahed Armaghani, D., Asteris, P. G., Askarian, B., Hasanipanah, M., Tarinejad, R., & Huynh, V. V. (2020). Examining hybrid and single SVM models with different kernels to predict rock brittleness. Sustainability, 12(6), 2229.
26. Daneshfaraz, R., Norouzi, R., Abbaszadeh, H., & Azamathulla, H. M. (2022). Theoretical and experimental analysis of applicability of sill with different widths on the gate discharge coefficients. Water Supply, 22(10), 7767-7781.
27. Abbaszadeh, H., Daneshfaraz, R., Sume, V., & Abraham, J. (2024). Experimental investigation and application of soft computing models for predicting flow energy dissipation in arc-shaped constrictions. AQUA—Water Infrastructure, Ecosystems and Society, 73(3), 637-661.
28. Daneshfaraz, R., Norouzi, R., Ebadzadeh, P., & Kuriqi, A. (2023). Influence of sill integration in labyrinth sluice gate hydraulic performance. Innovative Infrastructure Solutions, 8(4), 118.
29. Crookston, B. M., & Tullis, B. P. (2012). Labyrinth weirs: Nappe interference and local submergence. Journal of Irrigation and Drainage Engineering, 138(8), 757-765.